Proceedings of the 7th International Symposium on Cavitation
CAV2009 – Paper No. 60
August 17-22, 2009, Ann Arbor, Michigan, USA

Rate-Dependent Hydroelastic Response of Self-Adaptive Composite Propellers in Fully Wetted and Cavitating Flows

Yin Lu Young
Dept. of Naval Architecture & Marine Engineering
University of Michigan
Ann Arbor, MI, USA

Michael Motley
Dept. of Civil & Environmental Engineering
Princeton University
Princeton, NJ, USA

ABSTRACT

The objectives of this work are to investigate the fully wetted and cavitating performance of a self-adaptive composite propeller and its dependence on the propeller rotational frequency (RPM or revolution per minute) in addition to the advance coefficient and ambient pressure. Self-adaptive composite propellers are designed to take advantage of the intrinsic deformation coupling behavior of anisotropic composites to improve propeller performance via automatic, passive blade pitch adjustment in spatially or temporally varying flow. The design methodology, numerical and experimental studies of self-adaptive composite propellers in fully wetted flow can be found in [1-7]. In past studies, the primary focus was the fully wetted performance of the composite propellers operating at the design RPM. However, since the deformations of adaptive composite propellers depend on the hydrodynamic load, which in turn depends on the propeller RPM, the response of adaptive composite propellers depend on both the advance coefficient and RPM. Moreover, at high RPMs, composite propellers may be subject to resonant vibration failure due to the inherent flexibility needed to achieve the desired self-adaptive behavior, and due to the decrease in natural frequency caused by added mass effects. Hence, it is important to evaluate the rate-dependent behavior of self-adaptive composite propellers. It is also important to evaluate the cavitating performance of self-adaptive composite propellers since cavitation can lead to thrust breakdown, decrease in efficiency, as well as erosion and localized impact damage to the composite blades. In this work, a previously validated coupled boundary element method – finite element method (BEM-FEM) is used to analyze the rate-dependent response of self-adaptive composite propellers in fully wetted and cavitating flows. Implications of the rate-dependent behavior on the design and interpretation of experimental studies, particularly cavitation tunnel studies, are discussed.

INTRODUCTION

Conventional marine propellers are typically made of nickel-aluminum-bronze or manganese-aluminum-bronze alloys. The blades are designed to act as rigid bodies that rotate in the water, and the geometry definitions are optimized for a specific flow condition represented by the advance coefficient, J=V/nD. V is the advance speed, n is the propeller rotational frequency, and D is the propeller diameter. Metallic propellers are relatively simple to design and analyze because the hydrodynamic and structural responses can be calculated separately since the blades only undergo rigid body rotation. A consequence of this rigidity, however, is that when the flow environment deviates from the design condition, the efficiency of the rigid propeller decreases. This happens when the propeller is operating in spatially varying wake or in off-design conditions.

To improve the propeller performance in spatially varying wake or in off-design conditions without resorting to the use of active control devices/units, self-adaptive composite propellers can be used. Compared to metals, composites offer several advantages, including higher strength-to-weight and stiffness-to-weight ratios. In addition, the load-dependent bend-twist coupling behavior of anisotropic composites can be used to enable automatic, passive blade pitch adjustment to improve propeller performance in spatially varying flow or in off-design flow conditions.

Although much work exist in the aerospace and wind turbine industry in the use of deformation coupling behavior of anisotropic composites to improve rotor performance, relatively little published work exist in the marine industry. An experimental study by [8] showed that tip deflections of composite hydrofoils helped to delay cavitation due to reduced tip loading, but there was negligible influence on the overall lift and drag coefficients. The design, fabrication, and testing of a pair of rigid and self-adaptive composite propellers was presented in [1]. The results show that an adaptive propeller can achieve equivalent performance compared to its rigid counterpart at the design flow condition, and achieve higher efficiency and delayed cavitation at highly loaded off-design conditions. The design methodology of self-adaptive composite propellers can be found in [6,7], where numerical predictions using a coupled BEM-FEM solver [5,9] confirmed that a

properly designed self-adaptive composite propeller can achieve equal or better performance than its rigid counterpart in off-design flow conditions and in spatially varying wake [2-7]. Similar findings using other numerical methods can be found in [10-12].

Most studies thus far focus on the fully wetted performance of the composite propellers operating at the design RPM. However, the performance of adaptive composite propellers depends not only on the advance coefficient (J) and ambient pressure, but also on the RPM (n). To maintain a constant J=V/nD, when the advance speed (V) increases, the propeller RPM (n) needs to be increased proportionally. Consequently, the dimensional load acting on the blade increases, leading to an increase in elastic blade (bending and twisting) deformation, which in turn changes the propeller loading thru fluid-structure interaction. Similarly, the propeller loading and deformation response change when the RPM is decrease from the design value. Hence, contrary to rigid propellers where the performance depends only on J (assuming no change in submergence, shaft or yaw angle, etc), the performance of adaptive composite propellers depend on both J and RPM. Moreover, at high RPMs, composite propellers may be subject to resonant vibration failure because of the inherent flexibility needed to achieve the desired self-adaptive behavior, and due to the decrease in natural frequency caused by added mass effects.

Another problem when operating at high speeds is cavitation, which can lead to performance decay and erosion damage. To measure thrust breakdown caused by cavitation, a common practice is to carry out model-scale studies inside a cavitation tunnel, where the tunnel pressure can be adjusted to simulate different cavitation numbers, $\sigma_n=(P_o-P_v)/(0.5\rho n^2D^2)$. P_o is the pressure inside the cavitation tunnel, which can be adjusted to be equal to the absolute hydrostatic pressure in the ocean ($P_o=P_{atm}+\rho gh$, where h is the depth of the shaft axis from the free surface). P_v is the saturated vapor pressure of the fluid with density ρ. For each value of J, the V and n are usually fixed, and only P_o is varied to simulate different σ_n. Although such testing procedure is sufficient for a rigid metallic propeller, the rate dependence of an adaptive composite propeller introduces additional complexity. In reality, cavitation occurs because of increase in ship speed (achieved by increasing the engine RPM) for a fixed depth (i.e. fixed P_o), which leads to reduction in cavitation number. Since the performance of adaptive composite propellers depend on the dimensional load, both V and n should be changed to simulate different σ_n for each value of J. In other words, it is not appropriate to simply change P_o to achieve the same σ_n as the prototype without changing n; else, cavitation tunnel simulations will not correspond to reality.

OBJECTIVE

The objective of this work is to analyze the rate-dependent response of a self-adaptive composite propeller in fully wetted and cavitating flows using a previously validated BEM-FEM model and to discuss the implications of this behavior on cavitation tunnel studies. It should be mentioned that this study does not address the impact of cavitation collapse on laminated composites, which is important but beyond the scope of this paper.

METHODOLOGY

A coupled BEM-FEM model is used to simulate the hydroelastic response of both the rigid and adaptive propellers. The BEM solves for the perturbation velocity induced by the propeller by assuming the total inflow velocity to be composed of the effective inflow velocity and the perturbation potential velocity induced by the propeller. The effective inflow velocity is defined in a non-inertial, rotating, blade-fixed coordinate system and represents the velocity distribution at the rotor plane in absence of the rotor, the angular velocity of the rotor, and the vortical interactions between the rotor and the inflow.

Assuming that the effective inflow velocity is known via numerical simulations or experimental measurements, the fluid problem is reduced to a mixed, moving boundary value problem governed by the Laplace equation for perturbation velocity potential for incompressible, inviscid, irrotational flow. This problem is solved using a lower-order potential-based BEM by applying Green's third identity in the time domain. Viscous effects are considered by applying a friction coefficient over the wetted blade surfaces. The flow tangency condition is imposed on the wetted blade surfaces. On the cavitating surfaces, the pressure is required to be constant and equal to the saturated vapor pressure of the fluid. The wake sheet is assumed to have zero thickness and be aligned with the circumferentially averaged velocity using the method developed by [13]. The thicknesses of the cavities are determined by applying the flow tangency condition on the cavitating blade and wake surfaces. Details of the BEM can be found in [14,15].

Fluid-structure interaction effects are considered by linearly decomposing the perturbation velocity potential into a part due to rigid body rotation and a part due to elastic blade deformation. Pressure and velocity compatibility conditions are applied on the deforming blade surfaces to establish a relation for the transient hydroelastic force induced by the elastic body deformation in terms of an added mass matrix multiplied by the solid nodal acceleration vector and a hydrodynamic damping matrix multiplied by the solid nodal velocity vector [5,9]. These matrices are superimposed onto the structural mass and damping matrices via user-defined hydroelastic elements [5,9] and the commercial FEM solver ABAQUS/Standard [16] is used to solve the modified equation of motion in the time domain for the deformable blades in the rotating blade-fixed coordinates system. The blades are assumed to be fixed at the roots and a minimum of three layers of quadratic continuum elements are used across the blade thickness for isotropic material, and extra layers are used to represent anisotropic composite layups. Nonlinear elastic blade deformations are considered through iterations between the BEM and FEM models. A detailed discussion of the methodology of the BEM-FEM model can be found in [5,9].

PROBLEM SETUP

The rigid propeller geometry utilized herein is based on propeller 5474, a composite propeller manufactured by AIR Fertigung-Technologie GmbH. The geometric details are given

in [1,3]. The propeller was designed and tested in cooperation with the Naval Surface Warfare Center, Carderock Division. Propeller 5474 has a diameter of 0.61 m and was optimized for the design flow condition represented by J=0.66 at *n* = 780 rpm. The adaptive composite propeller blades are designed to match exactly the rigid blade geometry under the design flow condition in open water to achieve the design performance characteristics in uniform inflow. For demonstration purposes, the adaptive propeller is assumed to be made of Hexcel IM7-8552 carbon epoxy, and the fiber orientation and stacking sequence ($[30°/30°/90°/90°/30°]_s$) are determined by optimizing the bend-twist coupling while ensuring structural integrity [17]. As a means of comparison, results for a rigid metallic propeller constructed of aluminum material are also presented. The material properties of both the adaptive composite and rigid metallic propeller are shown in Table 1. Both propellers are assumed to be 0.61m in diameter.

Figure 1 shows the undeformed geometry as well as the deformed (loaded) geometry of the adaptive composite propeller under the design flow conditions. The undeformed geometry represents the manufactured geometry without any applied loads; the deformed geometry under the design flow conditions matches exactly with that of the rigid blade geometry.

RESULTS – FULLY WETTED PERFORMANCE

The predicted open-water thrust coefficient ($K_T=T/\rho n^2D^4$), torque coefficient ($K_Q=Q/\rho n^2D^4$), and efficiency ($\eta=(K_T/K_Q)(J/2\pi)$) of the rigid and adaptive propellers are compared in Fig. 2 and Table 2. T is the thrust and Q is the torque. The constant n case corresponds to when n is fixed at the design value of 780 rpm, while V is varied to achieve different J values. The variable n case corresponds to when V is fixed at the design value of 5.23 m/s, while n is varied to achieve different J values.

The variations of the tip pitch angle with J for both the rigid and adaptive propellers are shown in Fig. 3. Both propellers have a linearly varying pitch angle distribution so the tip pitch angle is a representative value. The pitch angle distribution of the rigid propeller and the undeformed adaptive propeller do not vary with J. However, the theoretical optimal pitch angle distribution does change with J. Under (normal forward) hydrodynamic loading, the adaptive blades are designed to de-pitch, which helps to bring the deformed pitch angle distribution closer to the theoretical optimal values at off-design conditions, i.e. J<0.66 or J>0.66.

As shown in Figs. 2 and 3, the rigid and the adaptive propellers produced the same performance (K_T, K_Q and η) and same deformed tip pitch angle at the design flow condition (J=0.66, n=780 rpm). When J increases, which corresponds to decreases in angle of attack, the deformed tip pitch angle of the adaptive propeller becomes higher than the rigid propeller (because of the reduced load and deformation), which results in higher K_T and K_Q. The vice versa is true when J decreases. The differences in performance between the rigid and adaptive propellers are greater for the case with constant V than for the case with constant n because the hydrodynamic and rotor inertial forces are proportional to n^2 [18]. Consequently, the efficiency improvement from the rigid propeller is less when the adaptive propeller operates in constant n conditions compared to constant V conditions. Nevertheless, for all cases shown, the efficiency (η) of the adaptive propeller is higher, and the variation in thrust and torque are more gradual, than the rigid propeller. This demonstrates that the performance of the adaptive propeller is rate-dependent, and is in general better than the rigid propeller in off-design conditions. It has already been shown in [6,7] that similar improvement in performance can be achieved behind wake inflow because the adaptive blade can automatically adjust its pitch distribution as it rotates in spatially varying flow. Hence, it will not be repeated here.

A concern with adaptive composite propellers, however, is the susceptibility to resonance. The first three mode shapes and corresponding frequencies in water are shown in Figure 4 for both the rigid and adaptive propellers. The fundamental natural frequency of the adaptive propeller in water is only 69 Hz, compared to 136 Hz if the blades were made of aluminum. Hence, it is important to make sure that the highest excitation frequency of the adaptive propeller is significantly less than the fundamental frequency in water to avoid resonance.

RESULTS – CAVITATING PERFORMANCE

To investigate the cavitating performance of adaptive composite propellers, results are shown in this section assuming the propellers to operate at a depth (h) of 1 m from the free surface in the ocean. The cavitation number is defined as $\sigma_n = (P_o–P_v)/(0.5\rho n^2D^2)$, where P_v = 2,340 Pa and ρ = 997.66 kg/m^3.

Figures 5-8 compare the predicted performance curves, tip pitch angle variations, cavitation patterns, and pressure contours, respectively, with σ_n for the rigid and adaptive propellers at the design J. Two test scenarios are shown. The first scenario (variable n) corresponds to the real operation condition of varying V and n together to achieve different σ_n while maintaining J=0.66. Hence, $P_o=P_{atm} + \rho gh$ with P_{atm} = 101,325 Pa and g = 9.8 m/s^2. Selected results for the first scenario are shown in the third column of Figs. 7 and 8, and are listed in rows 2-4 of Table 3. The second scenario (constant n) corresponds to typical thrust breakdown studies inside a cavitation tunnel where V and n are fixed, and the tunnel pressure (P_o) is changed to match the same set of σ_n at J=0.66. Selected results for the second scenario are shown in the second column of Figs. 7 and 8, and are listed in rows 5-7 of Table 3. The rigid propeller results are the same for both scenarios, and are shown in the first column of Figs. 7 and 8.

For the rigid and adaptive propellers in both test scenarios, the blade is fully wetted at σ_n=3.59 and J=0.66. As σ_n reduces, the performance drops because midchord back cavitation and leading edge face cavitation develop on the blades. Only the face side pressure contours are shown in Fig. 8 because the difference between the two scenarios is more noticeable.

For the adaptive propeller operating at constant n, the change in pitch decreases with σ_n because the hydrodynamic loads reduce with increasing cavitation volume. Consequently, the deformed tip pitch angle becomes increasingly higher than the rigid blade values, which lead to reduced face cavitation and slightly larger back supercavitation (see the last two figures in rows 2 and 3 in Figs. 7 and 8). The reduction in face

cavitation volume leads to higher K_T, K_Q and η for the adaptive propeller when compared to the rigid propeller.

For the adaptive propeller operating at variable n, the dimensional load increased when σ_n drop from 3.5 to 2.5 because of the increased in RPM while the cavitation volume is still relatively limited. Consequently, the deformed tip pitch angle of the adaptive propeller is lower than that of the rigid propeller, and so are K_T and K_Q. However, as σ_n drops lower, the reduction in load caused by significant increase in cavitation volume counteracts the effect of increases in n. Hence, the deformed tip pitch angles of the adaptive propeller operating at variable n are higher than the rigid propeller values, but lower than the values that correspond to the adaptive propeller operating at constant n scenario, which explains the lower K_T and K_Q. Nevertheless, since the propellers are operating at the design J, the efficiencies of the rigid and adaptive propellers are similar except for σ_n=0.40 for both scenarios.

Perhaps a more important issue for adaptive composite propellers is that, at very low cavitation numbers in the variable n scenario, the excitation frequency (which are multiples of the propeller RPM) can approach the natural frequency of the blade. The fundamental natural frequency of the adaptive propeller in water (ω_1) is only 69 Hz. When $n>\omega_1/3$, the blades may be subject to load fluctuations and amplifications caused by resonant vibration. Moreover, convergence of the BEM-FEM iterations becomes an issue due to excessive deformations. This effect can be observed in the convergence history of the maximum von Mises stresses for V=30 knots, n/ω_1=0.56 in Fig. 9. Hence, it is strongly recommended to keep $n< \omega_1/3$ to avoid resonance and instability issues.

In addition to the design J, it is also important to investigate the performance of the adaptive propeller compared to the rigid propeller at off-design conditions.

The variation of the performance curves, tip pitch angle, cavitation pattern, and pressure contours for the rigid and adaptive propellers operating at J=0.792 are shown in Figs. 10-13. Selected results for the adaptive and rigid propellers are respectively shown in the left and right sides of Figs. 12 and 13. The corresponding flow conditions are listed in rows 8-10 of Table 3. The deformed tip pitch angles are in general higher than the rigid blade values, and hence K_T and K_Q are also higher. The efficiencies are in general higher for the adaptive propeller because the deformed tip pitch angles are closer to the theoretical optimal values. The de-pitching action increases when σ_n decreases from 5.18 to 1.8 because of increases in n. As σ_n drops below 1.8, the load reduces because of significant increase in cavitation volume, which prevails over the effect of increases in n. Consequently, the deformed tip pitch angle increases for the adaptive propeller blade as σ_n drops below 1.8.

The variation of the performance curves, tip pitch angle, cavitation pattern, and pressure contours for the rigid and adaptive propellers operating at J=0.528 are shown in Figs. 14-17. Selected results for the adaptive and rigid propellers are respectively shown in the left and right sides of Figs. 16 and 17. The corresponding conditions are listed in rows 11-13 of Table 3. The deformed tip pitch angles are in general lower than the rigid blade values, and hence the back cavitation volume is smaller, but K_T and K_Q are lower. Across the full range of cavitation numbers shown for J=0.528, the efficiencies of the adaptive propeller are higher than the rigid propeller.

The predicted variation of maximum tip displacement and von Mises stress with V and n for the adaptive propeller are shown in Figs. 18 and 19, respectively. The deformation and stress magnitudes vary along lines of constant J because the dimensional load is rate dependent. Moreover, the deformation and stress magnitudes do not simply increase with V and n because the hydrodynamic loads reduce when significant cavitation develops at high RPMs.

CONCLUSION

The objective of this paper is to study the effects of load-dependency on the fully wetted and cavitating response of adaptive composite propellers. The results demonstrated that both the fully wetted and cavitating responses of adaptive composite propellers depend on the advanced coefficient and propeller RPM in addition to other parameters such as submergence, shaft and yaw angles, etc. By designing the adaptive composite propeller to match the geometry of the optimized rigid propeller at the design flow conditions, and by selecting the optimal material configuration to achieve the desired load-deformation characteristics, the performance of the adaptive propeller can be equal to or better than its rigid counterpart in both fully wetted and cavitating flows. This is because the adaptive blade can automatically adjust its pitch angle distribution according to changes in the relative inflow by taking advantage of the intrinsic bend-twist coupling behavior of anisotropic composites. The results also demonstrate the importance of the RPM or load-dependent hydroelastic response. Contrary to rigid propellers where the performance depends only on J (assuming no change in submergence, shaft or yaw angle, etc), the performance of adaptive composite propellers depend on both J and RPM because the deformations depend on the dimensional load. Ignoring the RPM-dependence can lead to large errors in the calculations of propeller thrust, torque, and efficiency. The studies suggest that when conducting experimental studies of adaptive composite propellers inside a cavitation tunnel, both RPM and V need to be varied instead of simply changing the tunnel pressure to match the cavitation number. Another important consideration related to the propeller RPM is the susceptibility of the blades or the propulsion system to resonance. Hence, it is crucial to determine the natural frequencies of the components and the system in water to ensure that they are significantly higher than the highest excitation frequencies. It is also crucial to evaluate the stress and deformation responses of the adaptive propeller to avoid excessive deformation, strength, stability or fatigue failures. It is important to note that this study did not consider the impact of cavitation collapse on the blade surfaces, which is an area that requires attention and future research.

ACKNOWLEDGMENTS

The authors are grateful to the Office of Naval Research and Dr. Ki-Han Kim (program manager) for their financial support through grant numbers N00014-08-1-0475 and N00014-09-1-0367. The first author would also like to

acknowledge the funding provided by the 2009 ONR-ASEE Faculty Fellow Program.

REFERENCES

[1] Chen, B., Neely, S., Michael, T., Gowing S., Szwerc, R., Buchler, D., and Schult, R. 2006, "Design, fabrication, and testing of pitch-adapting (flexible) composite propellers," *SNAME Propeller/Shafting Symposium*, Williamsburg, Virginia, USA.

[2] Young, Y.L., Michael, T.J., Seaver, M., and Trickey, S.T. 2006, "Numerical and experimental investigations of composite marine propellers," *26th Symposium on Naval Hydrodynamics*, Rome, Italy.

[3] Young Y.L and Liu Z. 2007, "Hydroelastic tailoring of composite naval propulsors," *26th International Conference on Offshore Mechanics and Arctic Engineering*, San Diego, California, USA.

[4] Young, Y.L., Liu, Z., and Motley, M.R. 2008, "Influence of Material Anistotropy on the Hydroelastic Behaviors of Composite Marine Propellers," *27th Symposium on Naval Hydrodynamics*, Seoul, Korea.

[5] Young, Y.L. 2008, "Fluid-Structure Interaction of Flexible Composite Marine Propellers," *Journal of Fluids and Structures*, 24, 799-818.

[6] Motley, M.R., Liu, Z., and Young, Y.L. 2009, "Utilizing Fluid-Structure Interactions to Improve Energy Efficiency of Composite Marine Propellers in Spatially Varying Wake," *Composite Structures*, 90, 304-313.

[7] Liu, Z. and Young, Y.L. 2009, "Utilization of bend-twist coupling for performance enhancement of composite marine propellers," *Journal of Fluids and Structures*, doi:10.1016/j.jfluidstructs.2009.04.005.

[8] Gowing, S., Coffin, P., and Dai, C. 1998, "Hydrofoil cavitation improvements with elastically coupled composite materials," *Proceedings of 25th American Towing Tank Conference*, Iowa City, IA, USA.

[9] Young, Y.L. 2007, "Time-dependent hydroelastic analysis of cavitating propellers," *Journal of Fluids and Structures*, 23, 269-295.

[10] Lin, H. and Lin, J. 1997, "Effect of stacking sequence on the hydroelastic behavior of composite propeller blades," *Eleventh International Conference on Composite Materials*, Gold Coast, Australia. Australian Composite Structures Society.

[11] Lee, Y. and Lin, C. 2004, "Optimized design of composite propeller," *Mechanics of Advanced Materials and Structures*, 11, 17-30.

[12] Lin, C. and Lee, Y. 2004, "Stacking sequence optimization of laminated composite structures using genetic algorithm with local improvement," *Composite Structures*, 63, 339-345.

[13] Greeley, D. and Kerwin, J. 1982, "Numerical methods for propeller design and analysis in steady flow," Trans. SNAME, 90, Series D, 415-453.

[14] Young, Y. L. and Kinnas, S. A. 2003, "Analysis of supercavitating and surface-piercing propeller flows via BEM," *Computational Mechanics*, 32, 269-280.

[15] Young, Y. L. and Kinnas, S. A. 2004, "Performance prediction of surface-piercing propellers," *Journal of Ship Research*, 48, 288-305.

[16] ABAQUS 2005, "ABAQUS Version 6.5 Documentation," ABAQUS, Inc., 1080 Main Street, Pawtucket, Rhode Island, USA.

[17] Liu, Z. 2008, "Transient analysis and design of composite structures in multi-phase flows," Ph.D. Thesis, Princeton University.

[18] Young, Y.L. 2009, "Dynamic Hydroelastic Scaling of Self-Adaptive Composite Rotors," *Composite Structures*, Under Review.

Material	E_1 (GPa)	E_2 (GPa)	G_{12} (GPa)	ν_{12}	ν_{21}	ρ (kg/m^3)
Hexcel IM7-8552	171.42	9.08	5.29	0.32	0.32	1500
Rigid Aluminum	73.0 (Isotropic)			0.33 (Isotropic)		2700

Table 1: Material properties of the 0.61 m diameter rigid and adaptive propellers.

J	V (m/s)	n (rpm)	$K_T - (K_T)_{rigid}$	$K_Q - (K_Q)_{rigid}$	$\eta - \eta_{rigid}$
0.528	4.184	780	-0.0156	-0.00258	0.00881
0.660	5.230	780	-0.0002	0	0.00025
0.792	6.276	780	0.0179	0.00275	0.01600
0.528	5.230	975	-0.0404	-0.00634	0.01835
0.660	5.230	780	-0.0002	0	0.00025
0.792	5.230	650	0.0308	0.00481	0.02335

Table 2: Tip pitch angle and efficiency comparison of the adaptive propeller with constant rotational frequency (rows 2-4) and constant flow velocity (rows 5-7) with respect to the rigid propeller.

J	V (m/s)	V (knots)	n (rpm)	σ_n	n/ω_n	$\eta - \eta_{rigid}$
0.660	5.14	10	767	3.59	0.19	-0.0002
0.660	7.71	15	1150	1.60	0.28	0.0047
0.660	15.42	30	2300	0.40	0.56	0.0608*
0.660	5.14	10	767	3.59	0.19	-0.0002
0.660	5.14	10	767	1.60	0.19	0.0073
0.660	5.14	10	767	0.40	0.19	0.1337
0.792	5.14	10	639	5.18	0.15	0.0263
0.792	7.71	15	958	2.30	0.23	0.0038
0.792	10.28	20	1278	1.29	0.31	0.0511
0.528	5.14	10	958	2.30	0.23	0.0183
0.528	6.17	12	1150	1.60	0.28	0.0176
0.528	7.71	15	1437	1.02	0.35	0.0173

Table 3: Matrix of selected test conditions used to examine the load-dependent hydroelastic response of adaptive composite propellers in axisymmetric, cavitating flows.

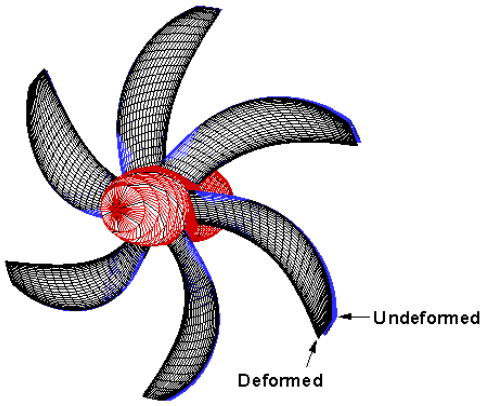

Figure 1: Undeformed and deformed geometries of the adaptive composite propeller under the design flow conditions.

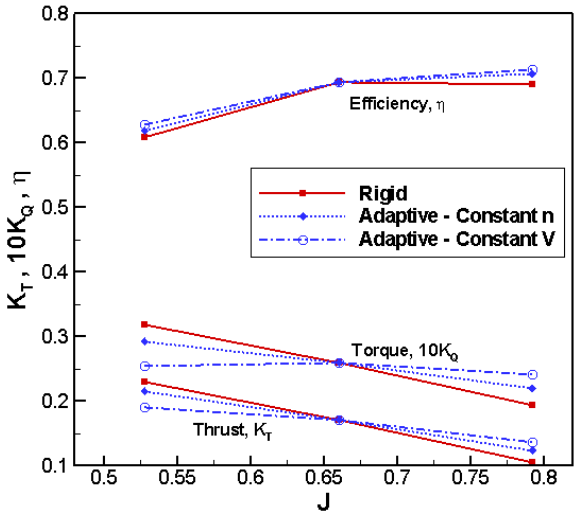

Figure 2: Comparison of the predicted open-water performance of the rigid and the adaptive propellers.

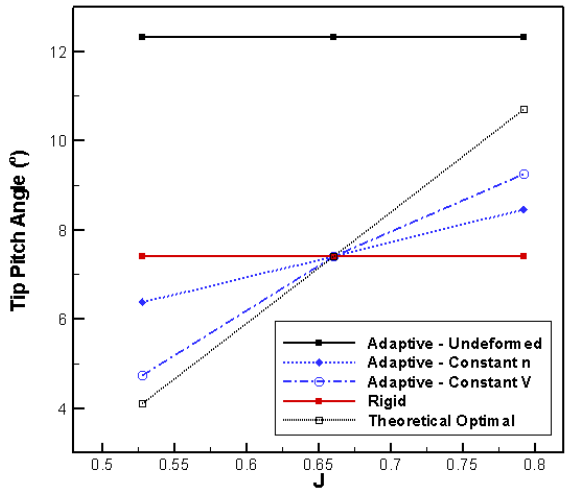

Figure 3: Predicted tip pitch angle variations of the adaptive propeller blade in open water flow.

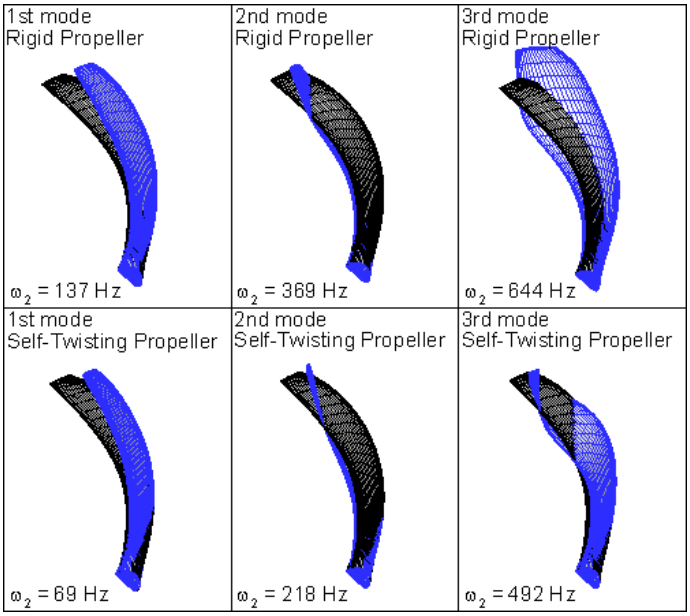

Figure 4: Comparison of the first three wetted mode shapes and wetted frequencies of both the rigid metallic and the adaptive composite propellers.

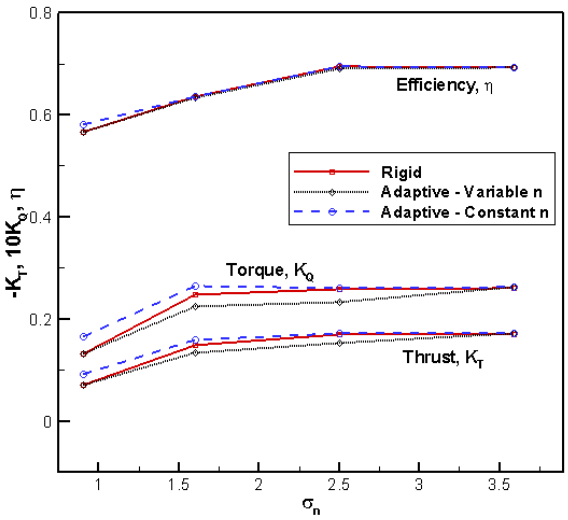

Figure 5: Comparison of the hydroelastic performance of the rigid and the adaptive propellers under variable and constant n conditions with varying cavitation number, σ_n, at J = 0.66.

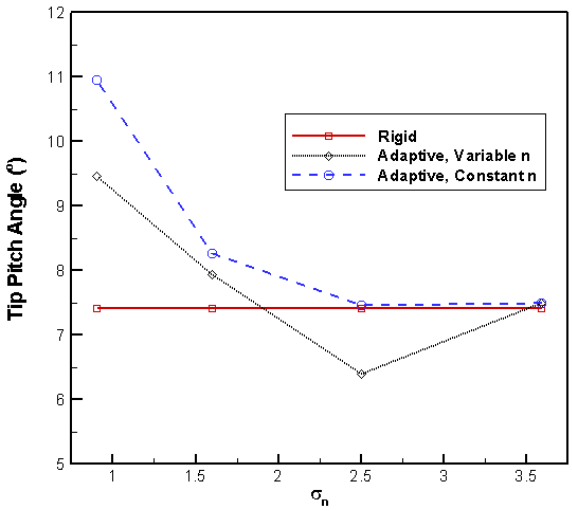

Figure 6: Comparison of the tip pitch angle of the rigid and the adaptive propellers under variable and constant n conditions with varying cavitation number, σ_n, at J = 0.66.

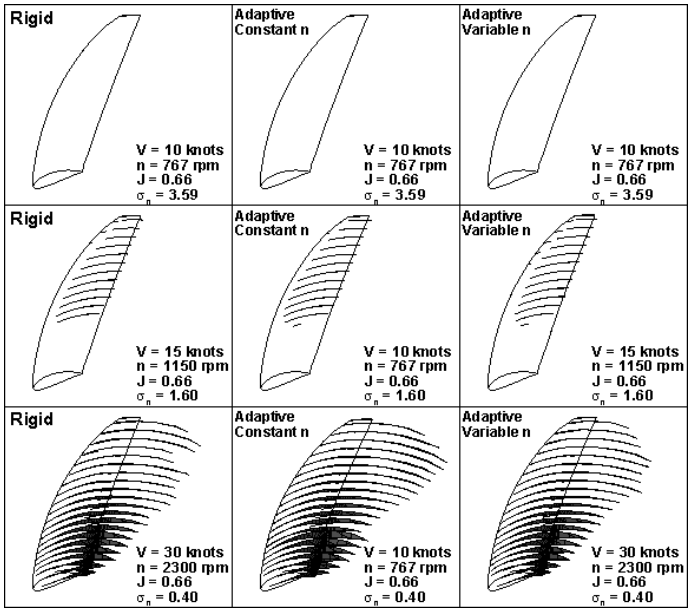

Figure 7: Predicted cavitation pattern for the rigid metallic (left column) propeller and adaptive composite propeller with constant RPM (middle column) and with variable RPM (right column) at J = 0.66.

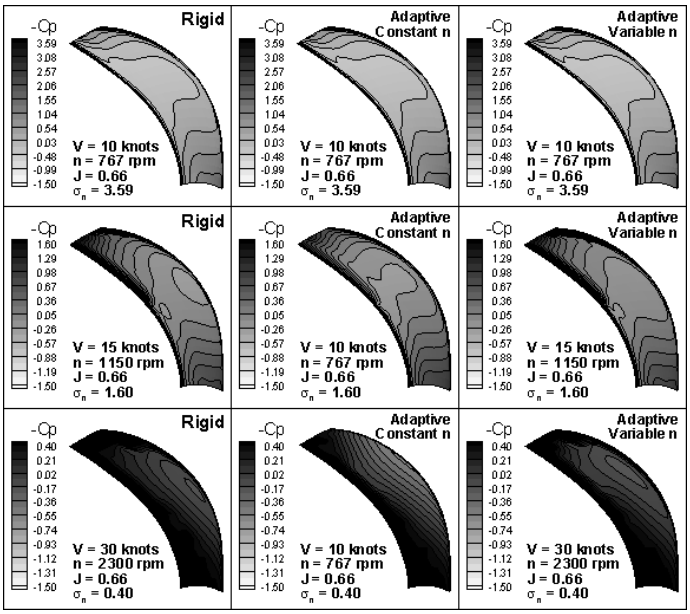

Figure 8: Predicted pressure contours for the rigid metallic (left column) propeller and adaptive composite propeller with constant RPM (middle column) and with variable RPM (right column) at J = 0.66.

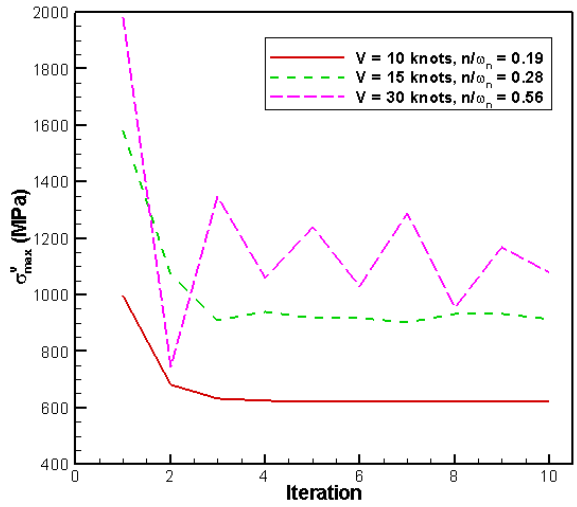

Figure 9: Convergence of the maximum von Mises stress for with number of BEM-FEM iterations for the adaptive composite propeller operating at J = 0.66.

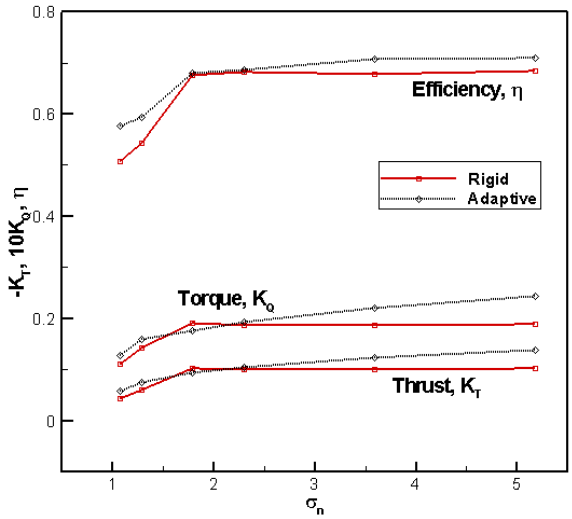

Figure 10: Comparison of the hydroelastic performance of the rigid and the adaptive propellers operating at variable n conditions with varying cavitation number, σ_n, at J = 0.792.

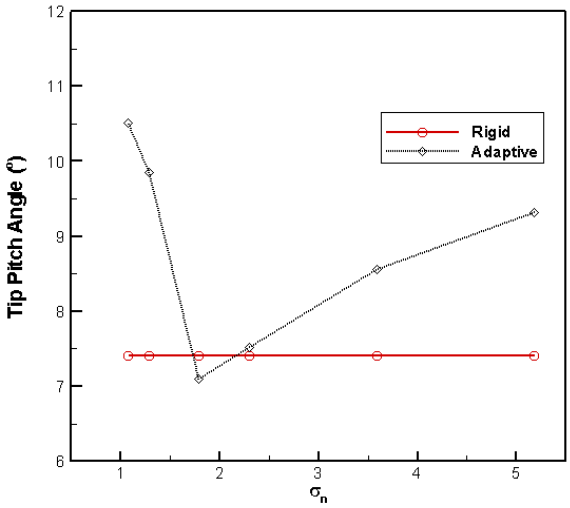

Figure 11: Comparison of the tip pitch angle of the rigid and the adaptive propellers operating under variable n conditions with varying cavitation number, σ_n, at J = 0.792.

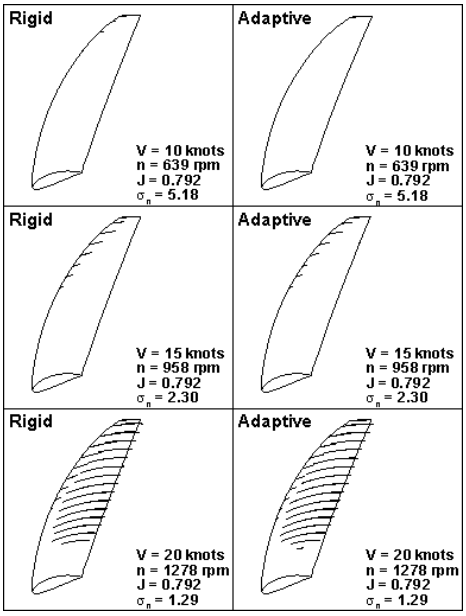

Figure 12: Predicted cavitation patterns for the rigid metallic (left column) propeller and adaptive composite propeller with variable rotational frequency (right column) at J = 0.792.

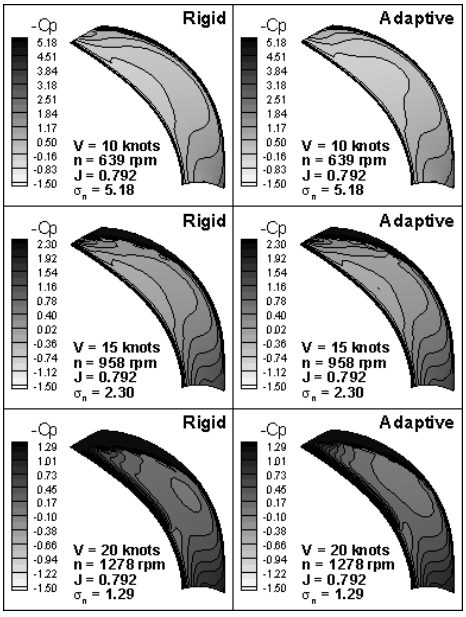

Figure 13: Predicted face side cavitation pressure distributions for the rigid metallic (left column) propeller and adaptive composite propeller with variable rotational frequency (right column) at J = 0.792.

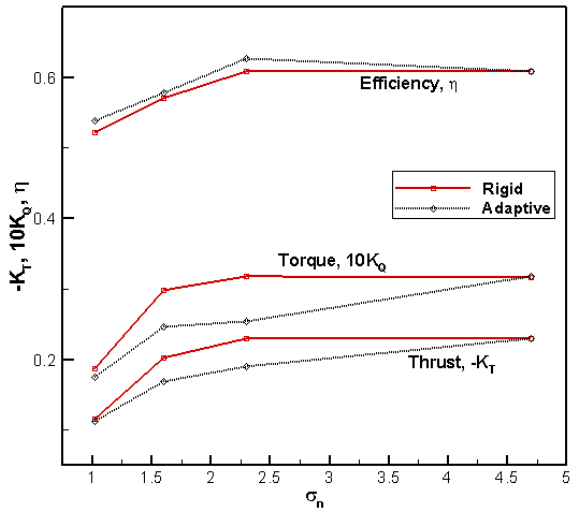

Figure 14: Comparison of the hydroelastic performance of the rigid and the adaptive propellers operating under variable n conditions with varying cavitation number, σ_n, at J = 0.528.

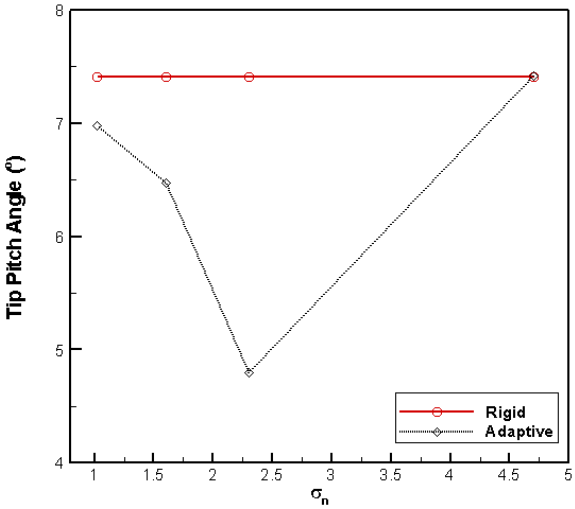

Figure 15: Comparison of the tip pitch angle of the rigid and the adaptive propellers operating under variable n conditions with varying cavitation number, σ_n, at J = 0.528.

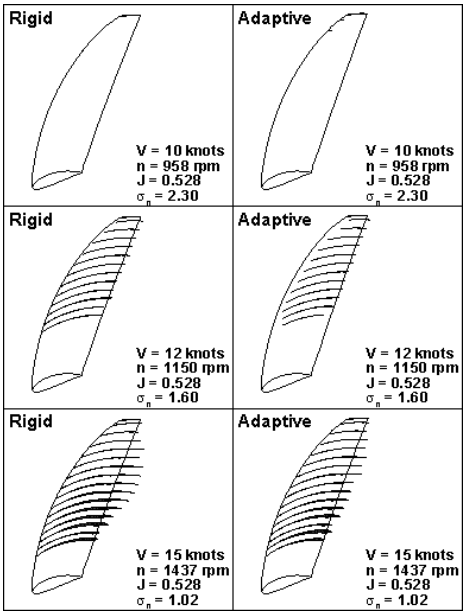

Figure 16: Predicted cavitation patterns for the rigid metallic (left column) propeller and adaptive composite propeller with variable rotational frequency (right column) at J = 0.528.

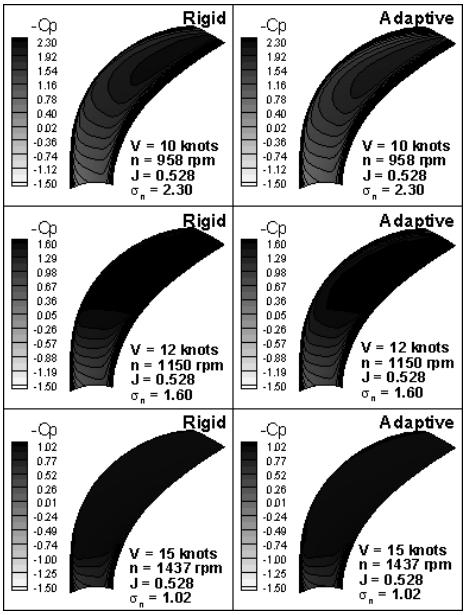

Figure 17: Predicted back side cavitation pressure distributions for the rigid metallic (left column) propeller and adaptive composite propeller with variable rotational frequency (right column) at J = 0.528.

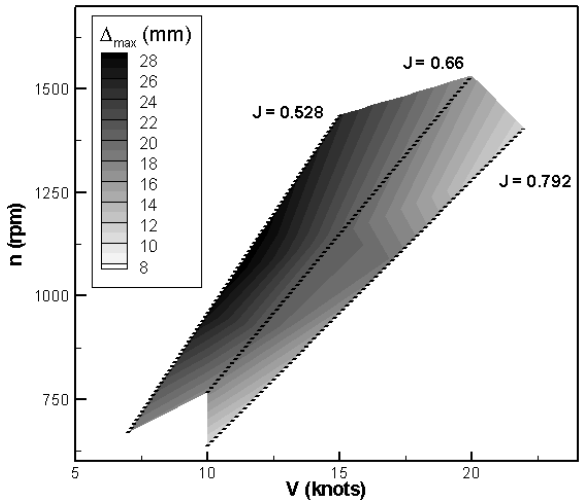

Figure 18: Predicted maximum displacement contours for the adaptive composite propeller over a range of flow conditions.

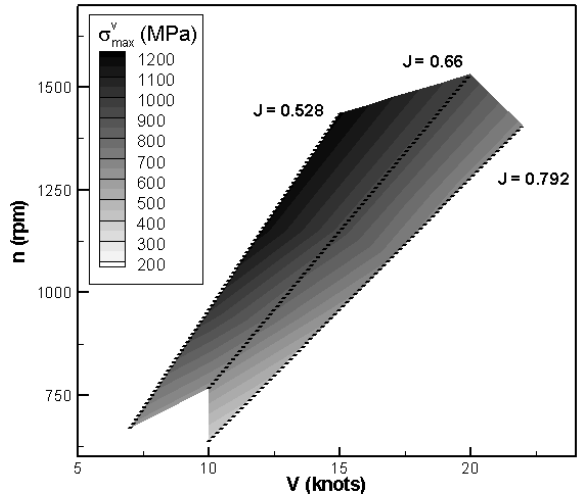

Figure 19: Predicted maximum von Mises stress contours for the adaptive composite propeller over a range of flow conditions.